Advanced models for free vibration analysis of laminated beams with compact and thin-walled open/closed sections

(Article begins on next page)

19 April 2024

Advanced models for free vibration analysis of laminated beams with compact and thin-walled open/closed sections

Erasmo Carrera[12*], Matteo Filippi[1†], Prashanta KR Mahato[13‡], Alfonso Pagani[a§]

[1]Department of Mechanical and Aerospace Engineering, Politecnico di Torino,
Corso Duca degli Abruzzi 24, 10129 Torino, Italy.

[2]King Abdulaziz University, Jeddah, Saudi Arabia.

[3]Department of Mechanical Engineering,
Indian School of Mines, Dhanbad-826004, India.

Author for correspondence:
E. Carrera, Professor of Aerospace Structures and Aeroelasticity,
Department of Mechanical and Aerospace Engineering,
Politecnico di Torino,
Corso Duca degli Abruzzi 24,
10129 Torino, Italy,
tel: +39 011 090 6836,
fax: +39 011 090 6899,
e-mail: erasmo.carrera@polito.it

---

[*]Professor of Aerospace Structures and Aeroelasticity, e-mail: erasmo.carrera@polito.it
[†]PhD student, e-mail: matteo.filippi@polito.it
[‡]Visiting Scholar, e-mail: prashanta.mahato@polito.it
[§]PhD student, e-mail:alfonso.pagani@polito.it

Abstract

In this paper, refined one-dimensional (1D) beam theories are implemented for the free vibration analysis of laminated beams with compact and thin-walled cross-sections. The proposed models are based on the Carrera Unified Formulation (CUF), which was formerly introduced for the analysis of plates and shells and recently expanded to beam structures by the first author and his co-workers. CUF is a hierarchical formulation leading to very accurate and computationally efficient finite element (FE) models. According to the latest developments in the framework of CUF, refined beam models are implemented using either Taylor-like or Lagrange-like polynomials in order to expand the unknown kinematic variables on the cross-section of the beam. Equivalent single layer models result from the former approach. On the other hand, if Lagrange polynomials are used, layer-wise models are produced. In this work, a classical 1D FE formulation along the beam length is used to develop numerical applications. A number of laminated beam structures are analysed and particular attention is given to laminated box beams with open and closed cross-section. The frequencies and the mode shapes obtained with the present refined beam elements are compared with solid/shell FE solutions from the commercial code MSC/Nastran and, when possible, with those found in the literature. The Modal Assurance Criterion (MAC) is used for model-to-model comparisons so as to demonstrate the enhanced capabilities of the proposed formulation in investigating the free vibration characteristics of both compact and thin-walled box laminated beams.

Introduction

The use of composite materials in various weight-sensitive structures (e.g. high speed aircraft, rocket, launch vehicles, etc.) is quite popular due to their well known attractive properties, such as high specific strength and stiffness, excellent fatigue and corrosion resistance. The wide use of laminated composite materials has aroused considerable interest in the related theoretical models and numerical simulation methods, including one-dimensional (1D) structural theories. Indeed, though the anisotropic materials exhibit a more complex behaviour than their metallic counterparts, the beam theories have been extensively used due to their simplicity and low computational costs. A considerable number of theories have been conceived in order to overcome the limitations of the first beam models introduced by Euler and Bernoulli [1] (hereinafter referred to as EBBM, i.e. Euler-Bernoulli Beam Model) and by Timoshenko [2] (hereinafter referred to as TBM, i.e. Timoshenko Beam Model) (see [3, 4]). For instance, Reddy [5] and Reddy and Khdeir [6] used parabolic distribution of the transverse shear strains in order to fulfill the free boundary condition for the shear stress on the top and bottom surfaces. Matsunaga [7] presented an higher-order model based on the method of power series expansion of displacement components along the depth coordinate z. Recently, Vidal et al. [8] proposed the approximation of the displacement field as a sum of separated functions of axial and transverse coordinate by adopting the Proper Generalized Decomposition (PGD) procedure, whereas Jun and Hongxing [9] used the Dynamic Stiffness Method (DSM) and a trigonometric shear deformation theory for solving the equations of motion of laminated beams. Furthermore, Grover et al. [10] studied the stability and the static behavior of laminated and sandwich plates by using an inverse hyperbolic shear deformation theory providing a closed-form solution for a simply supported symmetric plates while, in [11], Carrera compared different 2D theories in order to investigate the effects of the curvature and the shear deformation on buckling and vibrations of cross-ply laminated shells. As far as free vibration analyses are concerned, Subramanian [12] presented two different 1D finite elements (FEs) for laminated beams, in which the odd powers of the z-coordinate (until the 5th order) were used for expanding the axial displacement and the even powers were used for the transverse displacement (until the 4th order). In the paper by Marur and Kant [13], Taylor's series expansions were used for the axial displacement in order to describe the warping of cross-sections of sandwich and composite beams without the need of a shear correction factor. Interesting mixed formulations were presented in [14], where through-the-thickness continuity of transverse stress and displacement fields were enforced. Since frequently used in various engineering applications, Qatu *et al.* proposed new models for the study of curved beams performing on generally laminated structures both dynamic and static analyses ([15]-[16]). Furthermore, the authors provided a thorough review on the vibrations of curved and straight composite beams [17]. Other noteworthy contributions are those by Chen et al. [18], Stemple and Lee [19], Mitra et al. [20], Chandrashekhara et al. [21] and Chandrashekhara and Bangera [22]. The aforementioned theories based on the equivalent single layer (ESL) approach are not able to reproduce piecewise continuous displacement and transverse stress fields in the thickness direction, typical of the multilayered structures

3

[23, 24]. Hence, many researchers have adopted the layer-wise (LW) approach [25]. For instance, Shimpi and Ghugal [26] presented a new LW trigonometric model for two-layered cross-ply beams. Tahani [27] proposed two LW theories for analyzing the static and dynamic behavior of the laminated beams with a generic lamination. Surana and Nguyen [28] developed a 2D-beam element using Lagrange interpolating polynomials in the transverse direction to accurately describe the shear transverse stress distribution of composite curved structures. Despite the results being very accurate, the computational costs of the LW models rapidly grow when the number of the layers increases. For this reason, layer-independent theories that make use of zig-zag or Heaviside's through-the-thickness functions have been conceived. Murakami [29] was the first to introduce a zig-zag function into Reissner's mixed variational principle to develop an advanced plate theory (for a complete review about zig-zag methods, see [24]). Recently, Vidal and Polit [30, 31] presented a refined sine model for laminated beams by providing a Heaviside function for each layer to satisfy the continuity conditions for both displacements and transverse shear stress and the free conditions of the upper and lower surfaces. Subsequently, the same authors introduced Murakami's zig-zag function in the sine model [32] so as to take into account the discontinuity of the first derivative of the displacements. A further contribution was proposed in [33], where a new linear two-nodes beam element was evaluated based on the combination of classical TBM and a refined zig-zag theory.

Further theories have been developed for the studies of the lighter thin-walled box beams, see for example [34, 35, 36, 37, 38, 39, 40]. In the present paper, 1D higher-order theories based on generalized displacement variables are used to carry out free vibration analyses of laminated composite box beams. These theories are derived from the Carrera Unified Formulation (CUF) [41, 42]. Two classes of CUF 1D models were formulated in recent works: the Taylor-Expansion class, hereafter referred to as TE, and the Lagrange-Expansion class, hereafter referred to as LE. TE models exploit N-order Taylor-like polynomials to define the displacement field above the cross-section with N as a free parameter of the formulation. The strength of CUF TE beam models [43] in dealing with arbitrary geometries, thin-walled structures and local effects were evident in static [44, 45], free-vibration analysis [46, 47, 48] and asymptotic-like refined model analysis [49]. Recently, CUF TE theories were applied with reference to DSM to investigate the free vibration characteristics of isotropic [50] and laminated thin-walled structures [51]. Moreover, the dynamic analysis of laminated composite rotors were carried out in [52, 53, 54] through TE models. On the other hand, the LE class is based on Lagrange-like polynomials to discretize the cross-section displacement field and they have only pure displacement variables. Recently, static analyses on isotropic [55] and composite structures [56] have revealed the strength of LE models in dealing with open cross-sections, arbitrary boundary conditions and obtaining LW descriptions of the 1D model. Moreover, LE models have been successfully used for the component-wise analyses of both aeronautical [57, 58] and civil engineering structures [59, 60].

The main novelty of the present paper is that CUF models are extended to the free vibration analysis of composite thin-walled beams made of orthotropic layers that are arbitrarily rotated on the cross-sectional
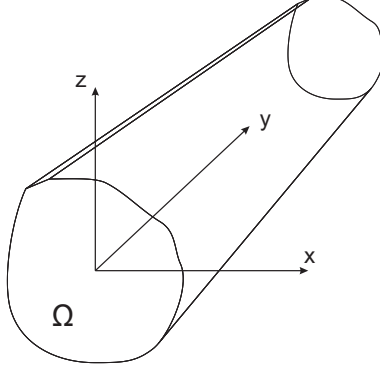
Figure 1. Coordinate frame of the beam model.

plane (xz-plane for the present reference system). In the next Section, CUF is introduced in the framework of the Finite Element Method (FEM). Then, numerical results by both TE and LE beam models are discussed and compared to those from the literature and by a commercial FEM code.

Unified formulation

Preliminaries

The adopted coordinate frame is presented in Figure 1. The beam boundaries over y are $0 \leq y \leq L$. The displacement vector is:

$$\mathbf{u}(x, y, z) = \left\{ \begin{array}{ccc} u_x & u_y & u_z \end{array} \right\}^T \tag{1}$$

Stress, $\boldsymbol{\sigma}$, and strain, $\boldsymbol{\epsilon}$, components are grouped as follows:

$$\boldsymbol{\sigma}_p = \left\{ \begin{array}{ccc} \sigma_{zz} & \sigma_{xx} & \sigma_{zx} \end{array} \right\}^T, \quad \boldsymbol{\epsilon}_p = \left\{ \begin{array}{ccc} \epsilon_{zz} & \epsilon_{xx} & \epsilon_{zx} \end{array} \right\}^T$$
$$\boldsymbol{\sigma}_n = \left\{ \begin{array}{ccc} \sigma_{zy} & \sigma_{xy} & \sigma_{yy} \end{array} \right\}^T, \quad \boldsymbol{\epsilon}_n = \left\{ \begin{array}{ccc} \epsilon_{zy} & \epsilon_{xy} & \epsilon_{yy} \end{array} \right\}^T \tag{2}$$

The subscript "n" stands for terms lying on the cross-section, while "p" stands for terms lying on planes which are orthogonal to Ω. Linear strain-displacement relations are used:

$$\epsilon_p = \boldsymbol{D}_p \mathbf{u}$$
$$\epsilon_n = \boldsymbol{D}_n \mathbf{u} = (\boldsymbol{D}_{n\Omega} + \boldsymbol{D}_{ny}) \mathbf{u} \tag{3}$$

5

with:

$$
\boldsymbol{D}_p = \begin{bmatrix} 0 & 0 & \frac{\partial}{\partial z} \\ \frac{\partial}{\partial x} & 0 & 0 \\ \frac{\partial}{\partial z} & 0 & \frac{\partial}{\partial x} \end{bmatrix}, \quad
\boldsymbol{D}_{n\Omega} = \begin{bmatrix} 0 & \frac{\partial}{\partial z} & 0 \\ 0 & \frac{\partial}{\partial x} & 0 \\ 0 & 0 & 0 \end{bmatrix}, \quad
\boldsymbol{D}_{ny} = \begin{bmatrix} 0 & 0 & \frac{\partial}{\partial y} \\ \frac{\partial}{\partial y} & 0 & 0 \\ 0 & \frac{\partial}{\partial y} & 0 \end{bmatrix}
\tag{4}
$$

The Hooke law is exploited:

$$
\boldsymbol{\sigma} = \tilde{\boldsymbol{C}}\boldsymbol{\epsilon}
\tag{5}
$$

According to Eq. 2, the Eq. 5 becomes:

$$
\begin{aligned}
\boldsymbol{\sigma}_p &= \tilde{\boldsymbol{C}}_{pp}\boldsymbol{\epsilon}_p + \tilde{\boldsymbol{C}}_{pn}\boldsymbol{\epsilon}_n \\
\boldsymbol{\sigma}_n &= \tilde{\boldsymbol{C}}_{np}\boldsymbol{\epsilon}_p + \tilde{\boldsymbol{C}}_{nn}\boldsymbol{\epsilon}_n
\end{aligned}
\tag{6}
$$

Box beams can be considered constituted by a certain number of straight orthotropic layers, whose material coordinate system $(1, 2, 3)$ generally do not coincide with the physical coordinate system (x, y, z) as shown in Figure 2. This figure also shows the capability of the present formulation to deal with arbitrary rotations of the fibres both in xy- and xz-planes. Using this approach, the matrices containing the coefficients of the generic material k are fully populated.

$$
\tilde{\boldsymbol{C}}_{pp}^k = \begin{bmatrix} \tilde{C}_{11}^k & \tilde{C}_{12}^k & \tilde{C}_{14}^k \\ \tilde{C}_{12}^k & \tilde{C}_{22}^k & \tilde{C}_{24}^k \\ \tilde{C}_{14}^k & \tilde{C}_{24}^k & \tilde{C}_{44}^k \end{bmatrix}, \quad
\tilde{\boldsymbol{C}}_{pn}^k = \begin{bmatrix} \tilde{C}_{15}^k & \tilde{C}_{16}^k & \tilde{C}_{13}^k \\ \tilde{C}_{25}^k & \tilde{C}_{26}^k & \tilde{C}_{23}^k \\ \tilde{C}_{45}^k & \tilde{C}_{46}^k & \tilde{C}_{43}^k \end{bmatrix}, \quad
\tilde{\boldsymbol{C}}_{nn}^k = \begin{bmatrix} \tilde{C}_{55}^k & \tilde{C}_{56}^k & \tilde{C}_{35}^k \\ \tilde{C}_{56}^k & \tilde{C}_{66}^k & \tilde{C}_{36}^k \\ \tilde{C}_{35}^k & \tilde{C}_{36}^k & \tilde{C}_{33}^k \end{bmatrix}
\tag{7}
$$

The explicit forms of the coefficients of the matrices $\tilde{\boldsymbol{C}}_{ij}^k$ are not given here for the sake of brevity, but they can be found in [54].

Hierarchical Higher-Order Models, TE and LE Classes

In the framework of CUF, the displacement field is the expansion of generic cross-sectional functions, F_τ

$$
\boldsymbol{u}(x, y, z) = F_\tau(x, z)\boldsymbol{u}_\tau(y) \qquad \tau = 1, 2, \ldots, M
\tag{8}
$$

where $\boldsymbol{u}_\tau$ is the vector of the *generalized* displacement, M is the number of terms of the expansion and, in according to the generalized Einstein's notation, τ indicates summation. The choice of F_τ determines the class of the 1D CUF model that has to be adopted. TE 1D models are based on polynomial expansions, $x^i z^j$, of the displacement field above the cross-section of the structure, where i and j are positive integers. For
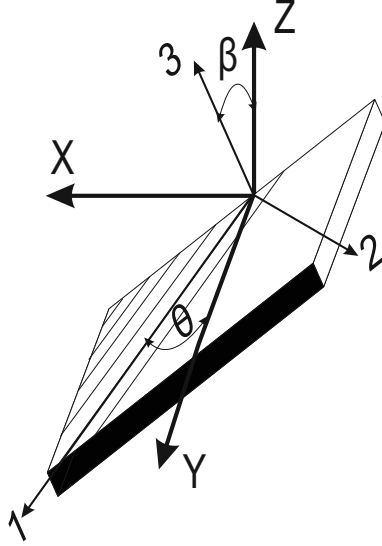
Figure 2. Physical and material reference systems.

instance, the displacement field of the second-order (N=2) TE model is expressed by

$$u_x = u_{x_1} + x\ u_{x_2} + z\ u_{x_3} + x^2\ u_{x_4} + xz\ u_{x_5} + z^2\ u_{x_6}$$

$$u_y = u_{y_1} + x\ u_{y_2} + z\ u_{y_3} + x^2\ u_{y_4} + xz\ u_{y_5} + z^2\ u_{y_6} \qquad (9)$$

$$u_z = u_{z_1} + x\ u_{z_2} + z\ u_{z_3} + x^2\ u_{z_4} + xz\ u_{z_5} + z^2\ u_{z_6}$$

The order N of the expansion is an input parameter of the analysis and defines the beam theory.

The LE class exploits Lagrange-like polynomials on the cross-section to build 1D higher-order models. The isoparametric formulation is exploited to deal with arbitrary shape geometries. In this paper, the nine-point (L9) cross-sectional polynomial set was adopted. For a L9 element (Figure 3), the interpolation functions are given by

$$F_\tau = \tfrac{1}{4}(r^2 + r\ r_\tau)(s^2 + s\ s_\tau) \qquad \tau = 1,3,5,7$$

$$F_\tau = \tfrac{1}{2}s_\tau^2(s^2 - s\ s_\tau)(1 - r^2) + \tfrac{1}{2}r_\tau^2(r^2 - r\ r_\tau)(1 - s^2) \qquad \tau = 2,4,6,8 \qquad (10)$$

$$F_\tau = (1 - r^2)(1 - s^2) \qquad \tau = 9$$

where r and s vary from -1 to $+1$, whereas r_τ and s_τ are the coordinates of the nine points whose locations
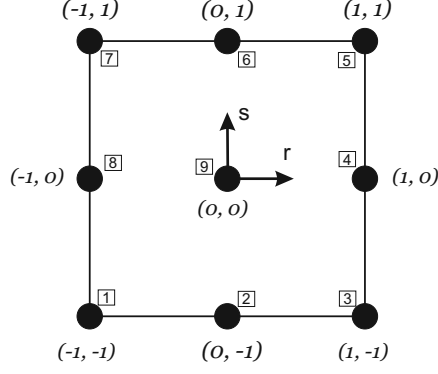
Figure 3. L9 element in the natural coordinate system.
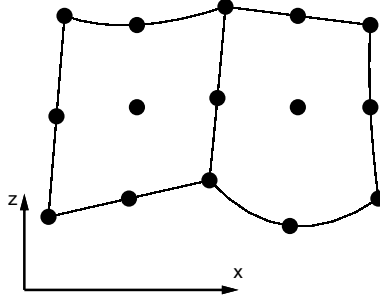
Figure 4. Two assembled L9 elements in actual geometry.

in the natural coordinate frame are shown in Figure 3. The displacement field of a L9 element is therefore

$$u_x = F_1 \ u_{x_1} + F_2 \ u_{x_2} + F_3 \ u_{x_3} + ... + F_9 \ u_{x_9}$$
$$u_y = F_1 \ u_{y_1} + F_2 \ u_{y_2} + F_3 \ u_{y_3} + ... + F_9 \ u_{y_9} \tag{11}$$
$$u_z = F_1 \ u_{z_1} + F_2 \ u_{z_2} + F_3 \ u_{z_3} + ... + F_9 \ u_{z_9}$$

where $u_{x_1}, ..., u_{z_9}$ are the displacement variables of the problem and they represent the translational displacement components of each of the nine points of the L9 element. According to [55], the beam cross-section can be discretized by using several L-elements for further refinements, as shown in Figure 4 where two L9 elements are assembled. This is one of the main feature of the LE approach, which clearly has LW capabilities as discussed in [56].

FE formulation

The FE approach was adopted to discretize the structure along the y-axis. The displacement field is given by:

$$\boldsymbol{u}(x, y, z) = N_i(y)F_\tau(x, z)\mathbf{q}_{\tau i} \tag{12}$$

where N_i stands for the shape functions and $\mathbf{q}_{\tau i}$ for the nodal displacement vector

$$\mathbf{q}_{\tau i} = \left\{ \begin{array}{ccc} q_{u_{x_{\tau i}}} & q_{u_{y_{\tau i}}} & q_{u_{z_{\tau i}}} \end{array} \right\}^T \tag{13}$$

For the sake of brevity, the shape functions are not reported here. They can be found in many books, for instance in [61]. The choice of the cross-section discretization for the LE class (i.e. the choice of the type, the number and the distribution of cross-sectional elements) or the theory order, N, for TE class is completely independent of the choice of the beam finite element to be used along the beam axis. In this work, 1D elements with four nodes (B4) were adopted, i.e. a cubic approximation along the y-axis was assumed.

The stiffness and mass matrices of the elements were obtained via the principle of virtual displacements

$$\delta L_{int} = \int_V (\delta \boldsymbol{\epsilon}_p^T \boldsymbol{\sigma}_p + \delta \boldsymbol{\epsilon}_n^T \boldsymbol{\sigma}_n) dV = -\delta L_{ine} \tag{14}$$

where L_{int} stands for the strain energy and L_{ine} is the work of the inertial loadings. δ stands for the virtual variation. The virtual variation of the strain energy is rewritten using Eq.s (3), (6) and (12)

$$\delta L_{int} = \delta \mathbf{q}_{\tau i}^T \mathbf{K}^{ij\tau s} \mathbf{q}_{sj} \tag{15}$$

where $\mathbf{K}^{ij\tau s}$ is the stiffness matrix in the form of the fundamental nucleus. In a compact notation, it can be written as

$$\begin{aligned}
\boldsymbol{K}^{ij\tau s} =\ & I_l^{ij} \triangleleft \left(\boldsymbol{D}_{np}^T F_\tau \boldsymbol{I} \right) \left[\tilde{\boldsymbol{C}}_{np}^k \left(\boldsymbol{D}_p F_s \boldsymbol{I} \right) + \tilde{\boldsymbol{C}}_{nn}^k \left(\boldsymbol{D}_{np} F_s \boldsymbol{I} \right) \right] + \\
& + \left(\boldsymbol{D}_p^T F_\tau \boldsymbol{I} \right) \left[\tilde{\boldsymbol{C}}_{pp}^k \left(\boldsymbol{D}_p F_s \boldsymbol{I} \right) + \tilde{\boldsymbol{C}}_{pn}^k \left(\boldsymbol{D}_{np} F_s \boldsymbol{I} \right) \right] \triangleright_\Omega + \\
& + I_l^{ij,y} \triangleleft \left[\left(\boldsymbol{D}_{np}^T F_\tau \boldsymbol{I} \right) \tilde{\boldsymbol{C}}_{nn}^k + \left(\boldsymbol{D}_p^T F_\tau \boldsymbol{I} \right) \tilde{\boldsymbol{C}}_{pn}^k \right] F_s \triangleright_\Omega \boldsymbol{I}_{\Omega y} + \\
& + I_l^{i,y j} \boldsymbol{I}_{\Omega y} \triangleleft F_\tau \left[\tilde{\boldsymbol{C}}_{np}^k \left(\boldsymbol{D}_p F_s \boldsymbol{I} \right) + \tilde{\boldsymbol{C}}_{nn}^k \left(\boldsymbol{D}_{np} F_s \boldsymbol{I} \right) \right] \triangleright_\Omega + \\
& + I_l^{i,y j,y} \boldsymbol{I}_{\Omega y} \triangleleft F_\tau \tilde{\boldsymbol{C}}_{nn}^k F_s \triangleright_\Omega \boldsymbol{I}_{\Omega y}
\end{aligned} \tag{16}$$

where

$$\boldsymbol{I}_{\Omega y} = \begin{bmatrix} 0 & 1 & 0 \\ 1 & 0 & 0 \\ 0 & 0 & 1 \end{bmatrix} \qquad \triangleleft \ldots \triangleright_\Omega = \int_\Omega \ldots d\Omega \tag{17}$$

$$\left(I_l^{ij}, I_l^{ij,y}, I_l^{i,y j}, I_l^{i,y j,y} \right) = \int_l \left(N_i N_j, N_i N_{j,y}, N_{i,y} N_j, N_{i,y} N_{j,y} \right) dy \tag{18}$$

For the sake of clearness, in Appendix A, the nine components of the fundamental nucleus of the matrix $\boldsymbol{K}^{ij\tau s}$

are written in explicit form.

The virtual variation of the work of the inertial loadings is

$$\delta L_{ine} = \int_V \rho \delta \mathbf{u}^T \ddot{\mathbf{u}} dV \tag{19}$$

where ρ^k stands for the density of the material and $\ddot{\mathbf{u}}$ is the acceleration vector. Equation (19) is rewritten using Eq. (12):

$$\delta L_{ine} = \delta \mathbf{q}_{\tau i}^T \mathbf{M}^{ij\tau s} \ddot{\mathbf{q}}_{sj} \tag{20}$$

where $\boldsymbol{M}^{ij\tau s}$ is the fundamental nucleus of the mass matrix. In compact form it can be written as:

$$\boldsymbol{M}^{ij\tau s} = I_l^{ij} \triangleleft (F_\tau \rho^k \boldsymbol{I} F_s) \triangleright \tag{21}$$

It should be noted that both $\boldsymbol{K}^{ij\tau s}$ and $\boldsymbol{M}^{ij\tau s}$ do not depend either on the expansion order or on the choice of the F_τ expansion polynomials. These are the key points of CUF that makes possible the straightforward formulation of any-order multiple class theories. In fact, the fundamental nuclei have to be expanded according to the indexes τ and s in order to obtain the elemental FE matrices of the arbitrary-order beam theory. The elemental matrices can then be assembled in the classical way of FEM by using beam nodes indexes i and j.

Once the global FE matrices are assembled, the undamped dynamic problem can be written as follows:

$$\mathbf{M}\ddot{\mathbf{q}} + \mathbf{K}\mathbf{q} = 0 \tag{22}$$

Introducing harmonic solutions, it is possible to compute the natural frequencies, ω_k, by solving an eigenvalues problem

$$(-\omega_k^2 \mathbf{M} + \mathbf{K})\mathbf{q}_k = 0 \tag{23}$$

where $\mathbf{q}_k$ is the kth eigenvector.

Results and Discussion

The proposed CUF beam formulations for laminated box beam structures is herein evaluated. The results from both TE and LE CUF models are compared to those from the literature and from the commercial code MSC/Nastran. Rectangular cross-section beams made of orthotropic layers were first analysed in order to assess the present methodology. Various stacking sequences and boundary conditions were considered. Unless differently specified, 10 B4 finite elements were used in the analysis for both TE and LE models to discretize
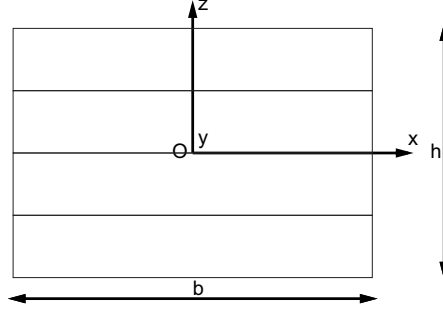
Figure 5. Rectangular cross-section of the graphite/epoxy 4-layer beam.

	Present CUF-LE		Present CUF-TE			Pagani et. al. [51]	Chen	Hodges	Exp.
	2 L9	4 L9	TBM	N=3	N=7	N=7	et. al.[18]	et. al. [63]	[62]
Mode 1[a]	85.615	85.493	116.410	85.649	85.349	85.295	82.55	77.346	82.5
Mode 2[b]	338.118	336.589	458.656	336.677	335.123	335.008	−*	307.26	−
Mode 3[a]	530.503	529.541	723.478	530.599	528.629	528.497	515.68	479.19	511.3
Mode 4[a]	1470.093	1465.008	1999.314	1470.528	1462.120	1460.747	1437.02	1317.3	1423.4
Mode 5[c]	1600.537	1532.286	−	1622.812	1515.057	1514.886	−	1476.0	1526.9
Mode 6[b]	2017.168	2003.166	2622.721	2003.659	1994.925	1994.300	−	1836.5	−

[a]: Flexural (plane yz)/torsional mode

[b]: Flexural on plane xy

[c]: Torsional mode

*: Not provided

Table 1. Natural frequencies (Hz) of the 15° graphite/epoxy beam with the lamination plane being the xy-plane.

the beam axis.

Graphite/epoxy cantilever rectangular beam

A cantilever rectangular beam made of orthotropic graphite/epoxy layers was considered for the preliminary assessment. The geometry of the cross-section is shown in Figure 5. The cross-section of the beam was a laminated solid rectangle with 4 plies having the same ply angles. The height of the cross-section, h, was 3.175 mm, the width, b, 12.7 mm and the length, L, 190.5 mm. The material properties were $E_1 = 129.138$ GPa, $E_2 = E_3 = 9.404$ GPa, $\nu_{12} = \nu_{13} = \nu_{23} = 0.3$, $G_{12} = 5.157$ GPa, $G_{13} = 4.304$ GPa, $G_{23} = 2.541$ GPa, and $\rho = 1550.07$ kg/m^3. The data were taken from [62] that contains experimental results with which the results by the present work can be compared. The same structure was considered over the years in different papers [63, 18] whose results are given in the following for comparison purpose.

The predicted values of the natural frequencies by the present LE as well as by lower- to higher-order TE models are shown in Table 1 in the case of 15° ply angle and lamination plane placed in the xy-plane. Classical TBM model is also considered. Coupled bending/torsional, torsional as well as pure bending modes show up in the first sixth natural modal shapes. The results are compared with Pagani et al. [51], Chen et. al. [18], Hodges et. al. [63] and experimental results [62]. Regarding the present LE modeling approach, two models are addressed and they differ in the cross-sectional discretization. In particular, 2 L9 and 4 L9 elements were used on the beam cross-section as shown in Figure 6.

In the second case, the lamination plane of the $[15°]_4$ beam was considered in the yz-plane. The cross-
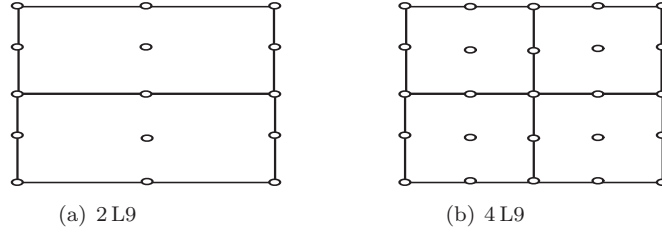
(a) 2 L9   (b) 4 L9

Figure 6. Cross-sectional L-element discretizations of the 4-layer laminated beam with the lamination plane being the xy-plane.
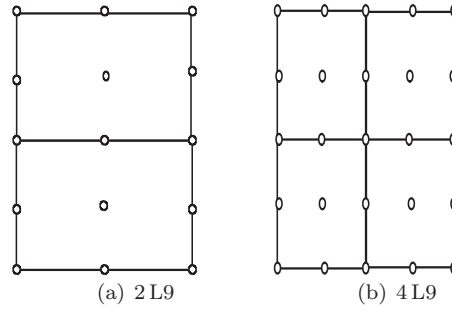

(a) 2 L9   (b) 4 L9

Figure 7. Cross-sectional L-element discretizations of the 4-layer laminated beam with the lamination plane being the the yz-plane.

section discretizations that were used for the two LE models are shown in Figure 7. Table 2 gives the first six natural frequencies of the laminated beam. As expected, it is observed that the frequencies are the same as in the previous case, i.e. when the laminate was in xy-plane. The following comments arise from the analysis:

- As expected, classical TBM is ineffective in detecting coupling and torsional modes. Pure bending natural frequencies are also overestimate.

- The results from both the LE and higher-order TE models are in good agreement with those from the

	Present CUF-LE		Present CUF-TE		
	2 L9	4 L9	TBM	N=3	N=7
Mode 1[a]	85.615	85.493	116.410	85.649	85.349
Mode 2[b]	338.118	336.589	458.656	336.677	335.123
Mode 3[a]	530.503	529.541	723.478	530.599	528.629
Mode 4[a]	1470.093	1465.008	1999.314	1470.528	1462.120
Mode 5[c]	1600.537	1532.286	—	1622.812	1515.057
Mode 6[b]	2017.168	2003.166	2622.721	2003.659	1994.925

[a]: Flexural (plane xy)/torsional mode

[b]: Flexural on plane yz

[c]: Torsional mode

Table 2. Natural frequencies (Hz) of the 15° graphite/epoxy beam with the lamination plane being the yz-plane.

| | Present CUF-LE | | Present CUF-TE | | | | Pagani et. al. [51] | Chen | Chandrashekhara |
	4 L9	8 L9	TBM	N=2	N=4	N=6	N=6	et. al.[18]	and Bangera [22]
Mode 1[a]	1.978	1.961	1.962	2.123	1.992	1.967	1.962	1.845	1.981
Mode 2[b]	2.022	1.990	2.051	2.154	2.098	2.061	2.045	—*	—
Mode 3[a]	5.168	5.129	5.185	5.577	5.199	5.007	5.134	4.987	5.217
Mode 4[b]	5.520	5.429	5.543	5.881	5.726	5.524	5.579	—	—
Mode 5[c]	9.309	9.160	—	10.344	9.251	9.137	9.131	—	—
Mode 6[a]	9.521	9.462	9.660	10.629	9.569	9.367	9.477	9.539	9.691
Mode 7[b]	10.679	10.493	10.591	11.379	11.071	10.752	10.782	—	—
Mode 8[a]	14.719	14.642	15.090	15.472	14.777	14.794	14.663	13.474	10.535
Mode 9[d]	15.149	15.002	15.175	16.093	15.338	15.389	15.092	15.292	15.098

[a]: Flexural on plane yz

[b]: Flexural on plane xy

[c]: Torsional mode

[d]: Axial/shear (plane yz) mode

*: Mode not provided by the theory

Table 3. Non-dimensional natural frequencies ($\omega^* = \frac{\omega L^2}{b}\sqrt{\frac{\rho}{E_{11}}}$) of the CC $[45°/-45°]_2$ laminated beam with the lamination plane being the xy-plane.

experimental tests and those by Chen et. al.[18], whose theory can unfortunately deal only with flexural modes in the plane perpendicular to the lamination plane.

- The results by Hodges et al. [63] slightly underestimate the natural frequencies according to experimental investigation and the present CUF models.

- Higher-order CUF beam models for laminated structures are effective in detecting coupled modes as well as pure bending and torsional modes.

- The proposed formulation is very accurate and capable of dealing with the rotation of the fibres not only in the xy-plane but also in yz-plane.

Angle-ply square cross-section beam

A square cross-section beam was further analyzed. An angle-ply $[45°/-45°]_2$ lamination scheme and clamped-clamped (CC) boundary conditions were considered. The beam had a square cross-section whose edges (b = h) were equal to 25.4 mm, while the length L was assumed to be 381 mm. The material data were $E_1 = 144.8$ GPa, $E_2 = E_3 = 9.65$ GPa; $\nu_{12} = \nu_{13} = \nu_{23} = 0.3$, $G_{12} = G_{13} = 4.14$ GPa, $G_{23} = 3.45$ GPa and $\rho = 1389.23$ kg/m^3.

Table 3 shows the main non-dimensional natural frequencies ($\omega^* = \frac{\omega L^2}{b}\sqrt{\frac{\rho}{E_{11}}}$) for the anti-symmetric angle-ply lamination scheme. The laminates were considered in the xy-plane for this analysis case. The results by the present LE and TE methods were compared to those from Pagani et. al. [51] and other works from the literature. As far as LE are concerned, two models are addressed in Table 3 differing on the number of the L9 elements on the cross-section. In the first case (4 L9), one L9 element was used for each layer. In the case of the 8 L9 LE model, a 4×4 cross-sectional distribution of L9 elements was adopted.

In the second analysis, the laminae were considered in the yz-plane and the non-dimensional natural frequencies from the present TE and LE beam models are listed in Table 4. For the case under consideration,

	Present CUF-LE		Present CUF-TE			
	4 L9	8 L9	TBM	N=2	N=4	N=6
Mode 1[a]	1.978	1.961	1.962	2.123	1.992	1.967
Mode 2[b]	2.022	1.990	2.051	2.154	2.098	2.061
Mode 3[a]	5.168	5.129	5.185	5.577	5.199	5.007
Mode 4[b]	5.520	5.429	5.543	5.881	5.726	5.524
Mode 5[c]	9.309	9.160	$-^*$	10.344	9.251	9.137
Mode 6[a]	9.521	9.462	9.660	10.629	9.569	9.367
Mode 7[b]	10.679	10.493	10.591	11.379	11.071	10.752
Mode 8[a]	14.719	14.642	15.090	15.472	14.777	14.794
Mode 9[d]	15.149	15.002	15.175	16.093	15.338	15.389

[a]: Flexural on plane xy

[b]: Flexural on plane yz

[c]: Torsional mode

[d]: Axial/shear (plane xy) mode

[*]: Mode not provided by the theory

Table 4. Non-dimensional natural frequencies ($\omega^* = \frac{\omega L^2}{b}\sqrt{\frac{\rho}{E_{11}}}$) of the CC $[45°/-45°]_2$ laminated beam with the lamination plane being the yz-plane.
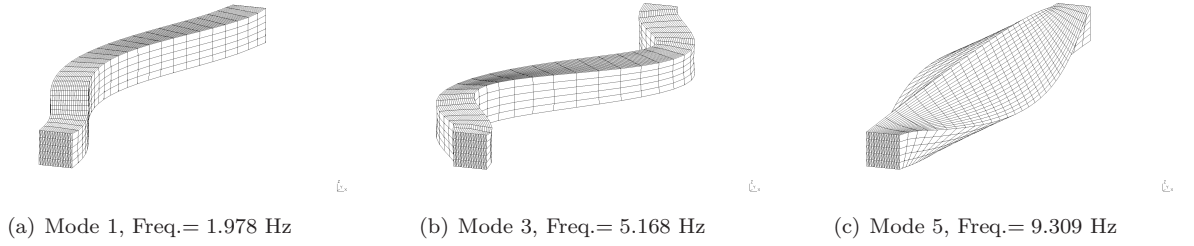

(a) Mode 1, Freq.= 1.978 Hz   (b) Mode 3, Freq.= 5.168 Hz   (c) Mode 5, Freq.= 9.309 Hz

Figure 8. Selected mode shapes of the CC $[45°/-45°]_2$ laminated beam with the lamination plane being the xy-plane. 8 L9 LE model.

some selected mode shapes by the 8 L9 LE beam model are shown in Figure 8. It should be emphasised that both TE and LE models are 1D and the mesh used in Figure 8 is merely a plotting grid for convenience used to show the 3D capabilities of the present approach. Some comments are noteworthy.

- The present LE and TE formulations are in good agreement with some theories from the literature, which can only deal with flexural modes in the plane perpendicular to the lamination plane.

- Classical TBM model gives good result for the problem under analysis since no coupling phenomena are evident.

- Various lamination schemes and arbitrarily rotated lamination planes can be analysed with the proposed approach.

Composite box beams

In this section a hollow rectangular cross-section laminated box beam was considered for verification. Clamped-free boundary conditions were addressed. The same structure was used for experimental [34] and analytical
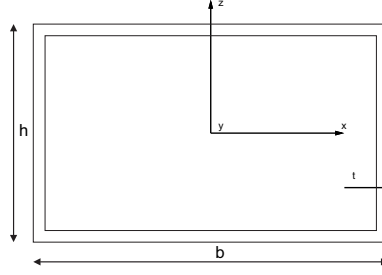
Figure 9. Cross-section of the laminated box beam.

Lay-up	Flanges		Webs	
	Top	Bottom	Left	Right
CAS2	$[30]_6$	$[30]_6$	$[30/-30]_3$	$[30/-30]_3$
CAS3	$[45]_6$	$[45]_6$	$[45/-45]_3$	$[45/-45]_3$
CUS1	$[15]_6$	$[-15]_6$	$[15]_6$	$[-15]_6$
CUS2	$[0/30]_3$	$[0/-30]_3$	$[0/30]_3$	$[0/-30]_3$
CUS3	$[0/45]_3$	$[0/-45]_3$	$[0/45]_3$	$[0/-45]_3$

Table 5. Various stacking sequences of the box beam used for comparison with previous works.

[35] investigations in previous works. The cross-section geometry is shown in Figure 9. The dimensions of the beam are as follows: length $L = 844.55$ mm, height $h = 13.6$ mm, width $b = 24.2$ mm and thickness $t = 0.762$ mm. The box beam was made of six layers with the following orthotropic material properties: $E_1 = 141.96$ GPa, $E_2 = E_3 = 9.79$ GPa, $\nu_{12} = \nu_{13} = 0.42$, $\nu_{23} = 0.5$, $G_{12} = G_{13} = 6.0$ GPa, $G_{23} = 4.83$ GPa, and $\rho = 1445.0$ kg/m^3. The six layers had the same thickness. Different lamination schemes are considered for the box beam under consideration. Both CAS (Circumferentially Asymmetric Stiffness) and CUS (Circumferentially Uniform Stiffness) stacking sequences are addressed and they are detailed in Table 5.

The values of the natural frequencies obtained from these box beam configurations are listed in Table 6, where the results from the present LE and TE models are compared to those from the literature. In particular, TBM, the third- and the seventh-order TE models as well as a LE model made with 24 L9 elements are compared to experimental data [34], analytical solutions [35] and a 2D FE model by ANSYS [40]. Regarding the 24 L9 model, it was obtained by using one single L9 element per layer on each flange and web. Both TE and LE models were discretized with 7 B4 elements along the axis for this analysis case.

To show the capability of the present models to deal with arbitrary lamination schemes, further ply angles for the CAS lay-up were considered. The variation of the first natural frequency versus fibre orientation angle by the present 24 L9 model are plotted in Figure 10 and compared with 2D FEM results from [40].

The following comments can be made:

- Classical TBM and lower-order TE models overestimate the natural frequencies of the proposed composite box beam.

- The present beam formulations can deal with both CAS and CUS lay-up box beam configurations. The results by the present LE and higher-order TE models are, in fact, in good agreement with those from

15

Lay-up	Mode	Present CUF-LE	Present CUF-TE			Exp.	Analytical	FEM
		24 L9	TBM	N=3	N=7	[34]	[35]	[40]
CAS2	1[a]	20.06	20.96	21.39	20.60	20.96	19.92	19.73
	2[b]	38.21	41.76	40.51	39.42	38.06	$-^{*}$	37.53
	3[a]	125.44	131.01	133.76	128.71	128.36	124.73	123.32
CAS3	1[a]	14.75	15.00	15.24	14.69	16.67	14.69	14.58
	2[b]	25.41	26.38	26.16	25.44	29.48	−	25.01
	3[a]	92.35	93.88	95.44	94.83	96.15	92.02	91.23
CUS1	1[a]	29.51	32.36	30.29	29.19	28.66	28.67	28.37
CUS2	1[a]	34.69	35.09	34.91	34.61	30.66	34.23	34.29
CUS3	1[a]	33.03	33.11	33.10	33.01	30.00	32.75	32.35

[a]: Flexural on plane yz

[b]: Flexural on plane xy

*: Not provided

Table 6. Natural frequencies (Hz) for different stacking sequences of the laminated box beam.
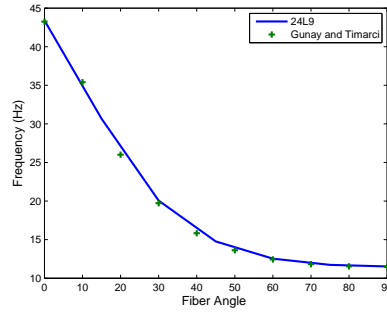

Figure 10. Variation of the fundamental frequency with respect to fibre orientation angle for CAS lay-up.
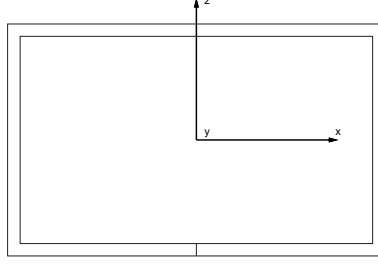
Figure 11. Open cross-section box beam.

analytical solutions and experimental data.

- Unlike the theory by Armanios and Badir [35], the present beam models can deal with bending modes in both yz- and xy-planes.

- Both LE and the seventh-order (N=7) TE models can detect the solution from a 2D shell FE model.

Laminated box beams with open and closed cross-section

The accuracy of the present beam formulations is further evaluated by considering a cantilever box with a [0/90] stacking sequence for the vertical edges and a [-45/+45] lamination for the horizontal edges. The lamination scheme of the box beam addressed is hereinafter referred to as the $[0/90/ - 45/ + 45]$ lay-up configuration. The cross-sectional dimensions of the structure are the same as in the previous case and open as well as closed cross-sections are considered. The open section is realized by considering a cut along the whole length of the beam as shown in Figure 11. The material properties were $E_1 = 69.0$ GPa, $E_2 = E_3 = 10.0$ GPa, $\nu_{12} = \nu_{13} = \nu_{23} = 0.25$, $G_{12} = G_{13} = G_{23} = 6$ GPa, $\rho = 2700$ kg/m^3.

The first ten natural frequencies and the number of degrees of freedom (DOFs) for each implemented model of the considered box beam both with and without the cut on the cross-section are listed in Table 7, where different aspect-ratio are accounted for. In Table 7 the results from the present LE modeling approach are compared to 3D FEM solutions from the commercial code MSC/Nastran. The Nastran solid models were obtained by using CHEXA 8-node brick elements, whereas 7 B4 cubic 1D finite elements were used along the axis in the case of LE models. Regarding the cross-sectional discretization, different LE configurations were considered and they are shown in Figure 12. In particular, the three LE models of the closed cross-section box beam were discretized with 8 L9, 16 L9 and 32 L9 elements (see Figure 12a,c-d). On the other hand, the open cross-section box beam was modeled with 10, 16 and 32 L9 elements as shown in Figure 12b-d. Unlike Figures 6 and 7, the cross-sectional Lagrange nodes are not depicted in Figure 12 for the sake of clearness. For both Nastran solid and LE models, the cut was realized by considering not-connected superimposed nodes in correspondence of the opening. TE models are not provided for this analysis case since they cannot successfully deal with cuts on the cross-section, as shown in [55] in the case of metallic beams. Some representative mode shapes of the closed and open cross-section laminated boxes are shown

17

L/b		Closed cross-section				Open cross-section			
		8 L9	16 L9	32 L9	Solid	10 L9	16 L9	32 L9	Solid
	DOFs	2640	5280	10560	1519200	3630	5610	10890	1533126
30	Mode 1	22.46	22.45	22.44	21.29	21.72	21.53	21.43	21.26
	Mode 2	29.85	29.82	29.79	29.15	22.42	22.40	22.40	22.38
	Mode 3	139.38	139.10	138.93	131.86	77.64	76.88	76.54	71.76
	Mode 4	184.30	183.77	183.57	179.78	124.13	123.59	123.29	124.26
	Mode 5	384.11	382.30	381.06	361.91	136.17	135.48	135.36	127.27
	Mode 6	504.17	475.89	466.92	463.72	322.15	313.56	312.72	293.81
	Mode 7	508.46	501.43	500.58	490.93	338.63	337.03	336.29	332.32
	Mode 8	736.19	728.61	722.80	687.43	412.37	405.68	403.81	388.89
	Mode 9	957.15	948.40	945.80	929.15	477.27	461.52	459.22	440.59
	Mode 10	1184.3	1160.30	1140.35	1086.90	542.34	497.57	495.83	493.45
20	Mode 1	50.44	50.39	50.36	47.78	46.15	45.87	45.71	47.07
	Mode 2	66.96	66.86	66.80	65.39	50.18	50.12	50.12	47.52
	Mode 3	309.12	307.80	306.97	291.45	161.51	160.25	159.78	151.91
	Mode 4	405.95	403.89	403.25	395.39	272.61	269.93	269.42	251.43
	Mode 5	764.88	710.76	696.47	690.16	275.33	271.41	270.87	270.33
	Mode 6	836.78	826.12	817.97	778.20	516.17	500.10	497.41	479.50
	Mode 7	1082.94	1071.59	1068.19	1049.99	546.18	501.62	499.69	497.68
	Mode 8	1565.56	1515.91	1473.13	1408.47	659.97	622.81	618.54	630.56
	Mode 9	1795.15	1794.38	1730.47	1625.87	741.68	732.55	718.76	667.46
	Mode 10	1994.08	1881.85	1793.92	1775.37	805.29	739.16	729.02	723.56
10	Mode 1	199.48	198.91	198.56	188.72	175.42	174.85	174.48	176.03
	Mode 2	263.54	262.69	262.35	257.32	188.80	186.97	186.96	176.05
	Mode 3	1152.80	1127.77	1108.52	1057.48	573.95	551.39	543.81	521.73
	Mode 4	1468.09	1375.85	1328.87	1294.29	592.99	558.23	558.72	552.94
	Mode 5	1543.05	1446.57	1439.44	1418.35	647.04	631.37	626.92	609.36
	Mode 6	2827.97	2407.52	2116.69	1934.45	1026.56	874.61	830.26	826.16
	Mode 7	3095.08	2606.73	2383.58	2223.94	1047.38	937.12	901.21	854.74
	Mode 8	3146.66	2772.29	2390.97	2320.44	1112.74	1037.29	1026.79	1004.57
	Mode 9	3210.37	3028.01	2631.67	2665.69	1414.34	1368.76	1306.61	1269.65
	Mode 10	3351.65	3075.56	2672.29	2708.97	1455.86	1373.35	1329.15	1303.31

Table 7. First ten natural frequencies (Hz) of the $[0/90/-45/+45]$ laminated box beam.
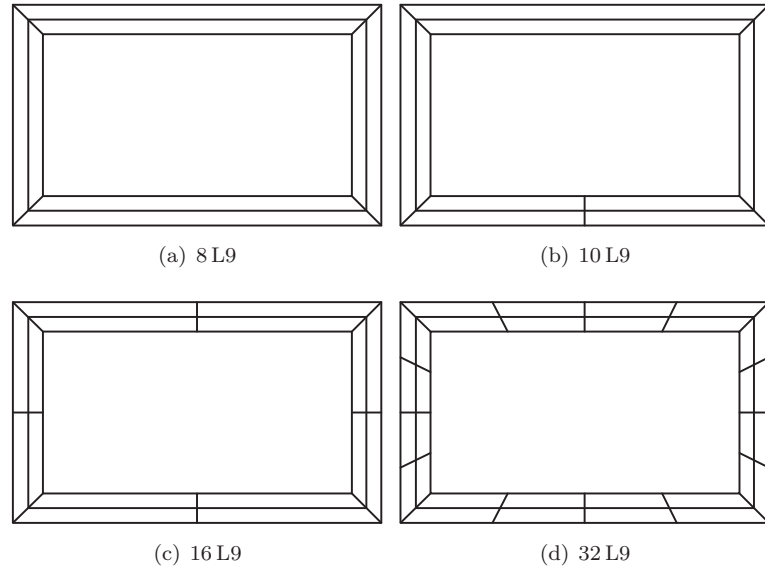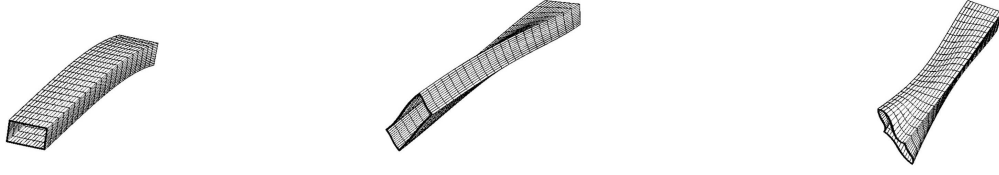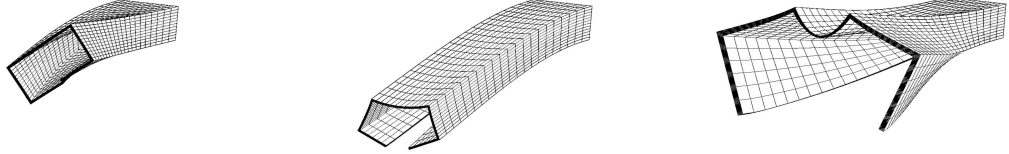

(a) 8 L9

(b) 10 L9

(c) 16 L9

(d) 32 L9

Figure 12. Cross-sectional discretization for the $[0/90/-45/+45]$ laminated box beam.

(a) Bending mode, Freq. = 198.91 Hz   (b) Torsional mode, Freq. = 403.89 Hz   (c) Shell-like mode, Freq. = 826.12 Hz

Figure 13. Selected mode shapes of the $[0/90/-45/+45]$ closed cross-section box beam. 16 L9 model, $L/b = 10$.

(a) Torsional mode, Freq.= 174.851 Hz   (b) Bending mode, Freq.= 186.97 Hz   (c) Opening mode, Freq.= 551.39 Hz

Figure 14. Selected mode shapes of the $[0/90/-45/+45]$ open cross-section box beam. 16 L9 model, $L/b = 10$.

in Figure 13 and 14, respectively. In particular bending, torsional, shell-like and opening modes are shown. Shell-like and opening modes notably demonstrate the capability of the present formulation in dealing with modal shapes involving large cross-sectional deformations.

The consistence correspondence between the 16 L9 LE model and the solid MSC/Nastran model was further investigated by means of the Modal Assurance Criterion (MAC) [64]. The MAC number is defined as a scalar representing the degree of consistency between two different modal vectors. MAC was formerly used for model-to-test comparisons and for model updating. However it can be successfully applied for model-to-model comparison as in [58]. The MAC takes on values from zero (representing no consistent correspondence) to one (representing a consistent correspondence) and it is defined as follows:

$$\text{MAC}_{ij} = \frac{|\{\phi_{A_i}\}^T \{\phi_{B_j}\}|^2}{\{\phi_{A_i}\}^T \{\phi_{A_i}\} \{\phi_{B_j}\} \{\phi_{B_j}\}^T} \tag{24}$$

where $\{\phi_{A_i}\}$ is the ith eigenvector of model A, while $\{\phi_{B_j}\}$ is the jth eigenvector of model B. Figures 15 and 16 represent the MAC values between the present LE model and the solid solution for different aspect ratios of the open and closed cross-section box beams. On the other hand, Figure 17 compares 8 L9 and the 16 L9 models in order to underline the fast convergence and to show that few L9 elements on the cross-section are enough to correctly detect the free vibration characteristics of laminated box beams. The following comments
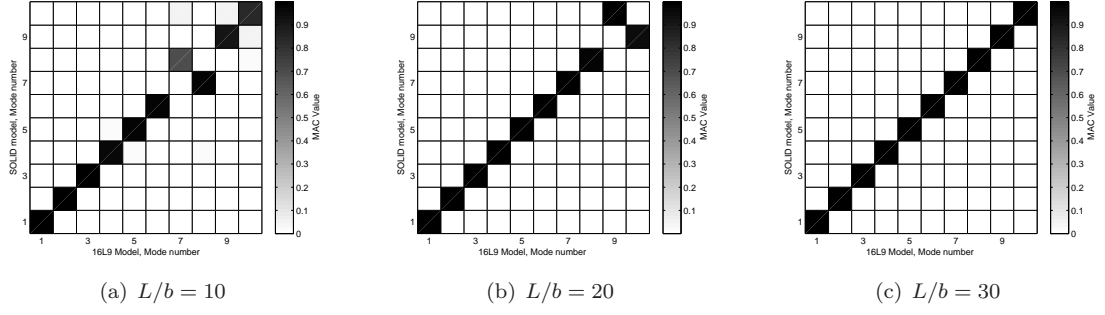
(a) $L/b = 10$ (b) $L/b = 20$ (c) $L/b = 30$

Figure 15. MAC values between 16 L9 and Nastran solid models of the $[0/90/-45/+45]$ closed cross-section box beam.
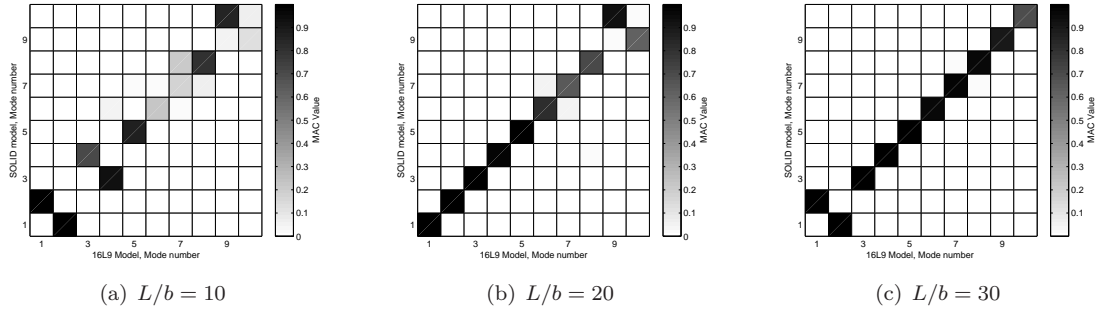

(a) $L/b = 10$ (b) $L/b = 20$ (c) $L/b = 30$

Figure 16. MAC values between 16 L9 and Nastran solid models of the $[0/90/-45/+45]$ open cross-section box beam.

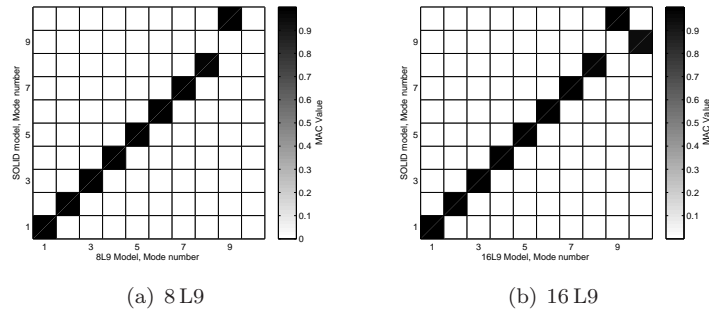
(a) 8 L9   (b) 16 L9

Figure 17. MAC values between 16 L9 and Nastran solid models of the $[0/90/-45/+45]$ closed cross-section box beam, $L/b = 20$.

arise:

- Both bending, torsional and coupled modes can be detected with the present LE models, in accordance with the Nastran solid solutions.

- Local modes characterized by large cross-sectional displacements appear as an opening cross-section is considered and they are correctly detected by the present LE approach.

- MAC analyses suggest a good correspondence in terms of modal behaviour between LE and MSC/Nastran solid models. Some differences are evident in the case of very short ($L/b = 10$) open cross-section since cross-sectional displacements are predominant.

- 1D LE models are very effective and they can deal with 3D solid-like solutions with very low computational costs.

Conclusion

In the present work, vibrational analysis of laminated composite structures was carried out by means of refined 1D models, and the results were compared to published literature and solid solutions from the commercial FEM code MSC/Nastran. Refined models foreseeing any rotation of the lamination plane on the beam cross-section have been developed by using the Carrera Unified Formulation (CUF), which is a hierarchical theory allowing for the straightforward implementation of 1D theories with arbitrary kinematics. According to CUF, the beam generalized degrees of freedom have been approximated on the beam cross-section through 2D polynomial functions in this paper. Depending on the choice of the polynomials, *global* Equivalent Single Layer (ESL) or *locally refined* Layer-Wise (LW) beam theories have been formulated. The former have been obtained by using Taylor-like polynomial expansions on the beam cross-section and this class of models have been referred to as TE (Taylor-Expansion). Conversely, LW theories have been produced by considering Lagrange polynomial approximations and they have been referred to as LE (Lagrange-Expansion). In this work, both TE and LE models have revealed their efficiency in the free vibration analysis of laminated compact and thin-walled box beams. Particularly, the attention has been focused the computational efficiency and the capability of the present LE to deal with solid-like solutions, even though large cross-sectional deformations are involved because of cuts and openings.

Future work will deal with the investigation of static and stress analyses of the laminated composite box beams via the proposed beam formulations.

References

1. L. Euler. *De curvis elasticis*. Lausanne and Geneva: Bousquet, 1744.

2. S. P. Timoshenko. On the transverse vibrations of bars of uniform cross section. *Philosophical Magazine*, 43:125–131, 1922.

3. K. Kapania and S. Raciti. Recent advances in analysis of laminated beams and plates, part I: Shear effects and buckling. *AIAA Journal*, 27(7):923–935, 1989.

4. K. Kapania and S. Raciti. Recent advances in analysis of laminated beams and plates, part II: Vibrations and wave propagation. *AIAA Journal*, 27(7):935–946, 1989.

5. J.N. Reddy. A simple higher–order theory for laminated composites. *Journal of Applied Mechanics*, 51:745–752, 1984.

6. J.N. Reddy and A.A. Khdeir. An exact solution for the bending of thin and thick cross-ply laminated beams. *Composite Structures*, 37:195–203, 1997.

7. H. Matsunaga. Interlaminar stress analysis of laminated composite beams according to global higher-order deformation theories. *Composite Structures*, 55:105–114, 2002.

8. P. Vidal, L. Gallimard, and O. Polit. Composite beam finite element based on the proper generalized decomposition. *Computers and Structures*, 102–103:76–86, 2012.

9. L. Jun and H. Hongxing. Dynamic stiffness analysis of laminated composite beams using trigonometric shear deformation theory. *Composite Structures*, 89:433–442, 2009.

10. N. Grover, D. K. Maiti, and B.N. Singh. A new inverse hyperbolic shear deformation theory for static and buckling analysis of laminated composite and sandwich plates. *Composite Structures*, 95:667–675, 2013.

11. E. Carrera. The effects of shear deformation and curvature on buckling and vibrations of cross-ply laminated composite shells. *Journal of Sound and Vibration*, 150(3):405–433, 1991.

12. P. Subramanian. Dynamic analysis of laminated composite beams using higher order theories and finite elements. *Composite Structures*, 73:342–353, 2006.

13. S. R. Marur and T. Kant. Free vibration analysis of fiber reinforced composite beams using higher order theories and finite element modelling. *Journal of Sound and Vibration*, 194(3):337–351, 1996.

14. M. Kameswara Rao, Y. M. Desai, and M. R. Chitnis. Free vibrations of laminated beams using mixed theory. *Composite Structures*, 52:149–160, 2001.

15. M.S. Qatu. Theories and analyses of thin and moderately thick laminated composite curved beams. *International Journal of Solids and Structures*, 30:2743–2756, 1993.

16. M. Hajianmaleki and M.S. Qatu. Static and vibration analyses of thick, generally laminated deep curved beams with different boundary conditions. *Composites: Part B*, 43:1767–1775, 2012.

17. M. Hajianmaleki and M.S. Qatu. Vibrations of straight and curved composite beams: A review. *Composites Structures*, 100:218–232, 2013.

18. Chen W.Q., C.F. Lv, and Z.G. Bian. Free vibration analysis of generally laminated beams via state-space-based differential quadrature. *Composite Structures*, 63:417–25, 2004.

19. A.D. Stemple and S.W. Lee. Large deflection static and dynamic finite element analysis of composite beams with arbitrary cross-sectional warping. *In: proceeding of the AIAA/ASME/ASCE/AHS/ASC 30th Structures, Structural Dynamics and Materials Conference*, Washington:1788–98, 1989.

20. M. Mitra, S. Gopalkrishan, and M.S. Bhat. A new superconvergent thin walled composite beam element for analysis of box beam structure. *Int. J. Solids Struct.*, 41:1491–518, 2004.

21. K. Chandrashekhara, K. Krishnamurthy, and S. Roy. Free vibration of composite beams including rotary inertia and shear deformation. *Computers and Structures*, 14:269–279, 1990.

22. K. Chandrashekhara and K.M. Bangera. Free vibration of composite beams using a refines shear flexible beam element. *Composite Structures*, 43(4):719–27, 1992.

23. N. J. Pagano. Exact solutions for composite laminates in cylindrical bending. *Journal of Composite Material*, 3:398–411, 1969.

24. E. Carrera. Historical review of zig-zag theories for multilayered plates and shells. *Applied Mechanics Reviews*, 9(2):287–308, 2002.

25. S.G. Lekhnitskii. *Anisotropic Plates*. 2nd Edition, Translated from the 2nd Russian Edited by SW Tsai and Cheron, Bordon and Breach, 1968.

26. R.P. Shimpi and Y.M. Ghugal. A new layerwise trigonometric shear deformation theory for two-layered cross-ply beams. *Composite Science and Technology*, 61:1271–1283, 2001.

27. M. Tahani. Analysis of laminated composite beams using layerwise displacement theories. *Composite Structures*, 79:535–547, 2007.

28. K.S. Surana and S.H. Nguyen. Two-dimensional curved beam element with higher-order hierarchical transverse approximation for laminated composites. *Composite Structures*, 36:499–511, 1990.

29. H. Murakami. Laminated composite theory with improved in-plane responses. *Jurnal of Applied Mechanics*, 53:661–666, 1986.

30. P. Vidal and O. Polit. A family of sinus finite elements for the analysis of rectangular laminated beams. *Composite Structures*, 84:56–72, 2008.

31. P. Vidal and O. Polit. Assessment of the refined sinus model for the non-linear analysis of composite beams. *Composite Structures*, 87:370–381, 2009.

32. P. Vidal and O. Polit. A sine finite element using a zig-zag function for the analysis of laminated composite beams. *Composites: Part B*, 42:1671–1682, 2011.

33. E.O. Oñate, A. Eijo, and S. Oller. Simple and accurate two-noded beam element for composite laminated beams using a refined zigzag theory. *Computer Methods in Applied Mechanics and Engineering*, 213–216:362–382, 2012.

34. R. Chandra and I. Chopra. Experimental-theoretical investigation of the vibration characteristics of rotating composite box beam. *J. Aircrafts*, 29(4):657–64, 1992.

35. E.A. Armanios and A.M. Badir. Free vibration analysis of anysotropic thin-wall close-section beams. *AIAA J*, 33(10):1905–10, 1995.

36. D. S. Dancila and E. A. Armanios. The influence of coupling on the free vibration of anisotropic thin-walled closed-section beams. *Internationl Journal of Solids and Structures*, 35(23):3105–3119, 1998.

37. Z. Qin and L. Librescu. On a shear-deformable theory of anisotropic thin-walled beams: further contribution and validations. *Composite Structures*, 56:345–358, 2002.

38. F. Shadmehri, H. Haddadpour, and M. A. Kouchakdeh. Flexural-torsional behavior thin walled composite beams with closed cross-section. *Thin-Walled Structures*, 45:699–705, 2007.

39. T. P. Vo and J. Lee. Free vibration of thin-walled composite box beam. *Composite Structures*, 84:11–20, 2008.

40. M.G. Gunay and T. Timarci. Free vibration of composite box-beams by ANSYS. In *International Scietific Conference (UNITECH)*, Gabrovo, Bulgaria, 16-17 November 2012.

41. E. Carrera. Theories and finite elements for multilayered, anisotropic, composite plates and shells. *Archives of Computational Methods in Engineering*, 56(3):87–140, 2003.

42. E. Carrera. Theories and finite elements for multilayered plates and shells: a unified compact formulation with numerical assessment and benchmarking. *Archives of Computational Methods in Engineering*, 10(3):216–296, 2003.

43. E. Carrera, G. Giunta, and M. Petrolo. *Beam Structures: Classical and Advanced Theories*. John Wiley & Sons, 2011. DOI: 10.1002/9781119978565.

44. E. Carrera, G. Giunta, P. Nali, and M. Petrolo. Refined beam elements with arbitrary cross-section geometries. *Computers and Structures*, 88(5–6):283–293, 2010. DOI: 10.1016/j.compstruc.2009.11.002.

45. E. Carrera, M. Petrolo, and E. Zappino. Performance of cuf approach to analyze the structural behavior of slender bodies. *Journal of Structural Engineeing*, 138(2):285–297, 2012.

46. E. Carrera, M. Petrolo, and P. Nali. Unified formulation applied to free vibrations finite element analysis of beams with arbitrary section. *Shock and Vibrations*, 18(3):485–502, 2011.

47. E. Carrera, M. Petrolo, and A. Varello. Advanced beam formulations for free vibration analysis of conventional and joined wings. *Journal of Aerospace Engineering*, 25(2):282–293, 2012.

48. E. Carrera, M. Filippi, and E. Zappino. Free vibration analysis of thin-walled cylinders reinforced with longitudinal and transversal stiffeners. *Journal of Vibration and Acoustics - ASME DC*, 135(1), 2012. DOI: 10.1115/1.4007559.

49. E. Carrera and M. Petrolo. On the effectiveness of higher-order terms in refined beam theories. *Journal of Applied Mechanics*, 78(3):041012(1–15), 2010.

50. A. Pagani, M. Boscolo, J.R. Banerjee, and E. Carrera. Exact dynamic stiffness elements based on one-dimensional higher-order theories for free vibration analysis of solid and thin-walled structures. *Journal of Sound and Vibration*, 332(23):6104–6127, 2013. DOI: 10.1016/j.jsv.2013.06.023.

51. A. Pagani, E. Carrera, M. Boscolo, and J.R. Banerjee. Refined dynamic stiffness elements applied to free vibration analysis of generally laminated composite beams with arbitrary boundary conditions. *Composite Structures*, 110:305–316, 2014.

52. E. Carrera, M. Filippi, and E. Zappino. Analysis of rotor dynamic by one-dimensional variable kinematic theories. *Journal of Engineering for Gas Turbines and Power - ASME DC*, 135(9):092501–09, 2013.

53. E. Carrera, M. Filippi, and E. Zappino. Free vibration analysis of rotating composite blades via Carrera Unified Formulation. *Composite Structures*, 106:317–325, 2013. DOI: 10.1016/j.compstruct.2013.05.055.

54. E. Carrera and M. Filippi. Variable kinematic one-dimensional finite elements for the analysis of rotors made of composite materials. *Journal of Engineering for Gas Turbines and Power - ASME*, 2014. DOI: 10.1115/1.4027192.

55. E. Carrera and M. Petrolo. Refined beam elements with only displacement variables and plate/shell capabilities. *Meccanica*, 47(3):537–556, 2012. DOI: 10.1007/s11012-011-9466-5.

56. E. Carrera and M. Petrolo. Refined one-dimensional formulations for laminated structure analysis. *AIAA Journal*, 50(1):176–189, 2012. DOI: 10.2514/1.J051219.

57. E. Carrera, A. Pagani, and M. Petrolo. Classical, refined and component-wise theories for static analysis of reinforced-shell wing structures. *AIAA Journal*, 51(5):12551268, 2013. DOI: 10.2514/1.J052331.

58. E. Carrera, A. Pagani, and M. Petrolo. Component-wise method applied to vibration of wing structures. *Journal of Applied Mechanics*, 80:041012, 2013. DOI: 10.1115/1.4007849.

59. E. Carrera, A. Pagani, and M. Petrolo. Refined 1D finite elements for the analysis of secondary, primary and complete civil engineering structures. *Journal of Structural Engineering*, 2014. DOI: 10.1061/(ASCE)ST.1943-541X.0001076.

60. E. Carrera and A. Pagani. Free vibration analysis of civil engineering structures by component-wise models. *Journal of Sound and Vibration*, 2014. DOI: 10.1016/j.jsv.2014.04.063.

61. K.J. Bathe. *Finite element procedure*. Prentice hall, 1996.

62. R.B. Abarcar and P. Cuniff. The vibration of cantilever beams of fiber reinforced material. *Composite material*, 10(16):504–17, 1972.

63. D.H. Hodge, A.R. Atilgan, M.V. Fulton, and L.W. Rehfield. Free vibration analysis of composite beams. *Journal of the American Helicopter Society*, 36(3):36–47, 1991.

64. R. J. Allemang and D. L. Brown. A correlation coefficient for modal vector analysis. In *Proceedings of the International Modal Analysis Conference*, pages 110–116, 1982.

Appendix A

For a cross-section made of non-homogeneous orthotropic material, the components of the fundamental nucleus $\boldsymbol{K}^{ij\tau s}$ are here written:

$$
\begin{aligned}
K_{xx} = \quad & I_l^{i,yj} \triangleleft F_\tau \tilde{C}_{46} F_{s,z} \triangleright \;+\; I_l^{i,yj} \triangleleft F_\tau \tilde{C}_{26} F_{s,x} \triangleright \;+\; I_l^{i,yj,y} \triangleleft F_\tau \tilde{C}_{66} F_s \triangleright \;+ \\
& I_l^{ij} \triangleleft F_{\tau,z} \tilde{C}_{44} F_{s,z} \triangleright \;+\; I_l^{ij} \triangleleft F_{\tau,z} \tilde{C}_{24} F_{s,x} \triangleright \;+\; I_l^{ij,y} \triangleleft F_{\tau,z} \tilde{C}_{46} F_s \triangleright \;+ \\
& I_l^{ij,y} \triangleleft F_{\tau,x} \tilde{C}_{26} F_s \triangleright \;+\; I_l^{ij} \triangleleft F_{\tau,x} \tilde{C}_{24} F_{s,z} \triangleright \;+\; I_l^{ij} \triangleleft F_{\tau,x} \tilde{C}_{22} F_{s,x} \triangleright
\end{aligned}
$$

$$
\begin{aligned}
K_{xy} = \quad & I_l^{i,yj} \triangleleft F_\tau \tilde{C}_{66} F_{s,x} \triangleright \;+\; I_l^{i,yj} \triangleleft F_\tau \tilde{C}_{56} F_{s,z} \triangleright \;+\; I_l^{i,yj,y} \triangleleft F_\tau \tilde{C}_{36} F_s \triangleright \;+ \\
& I_l^{ij} \triangleleft F_{\tau,x} \tilde{C}_{26} F_{s,x} \triangleright \;+\; I_l^{ij} \triangleleft F_{\tau,x} \tilde{C}_{25} F_{s,z} \triangleright \;+\; I_l^{ij} \triangleleft F_{\tau,z} \tilde{C}_{46} F_{s,x} \triangleright \;+ \\
& I_l^{ij} \triangleleft F_{\tau,z} \tilde{C}_{45} F_{s,z} \triangleright \;+\; I_l^{ij,y} \triangleleft F_{\tau,z} \tilde{C}_{43} F_s \triangleright \;+\; I_l^{ij,y} \triangleleft F_{\tau,x} \tilde{C}_{23} F_s \triangleright
\end{aligned}
$$

$$
\begin{aligned}
K_{xz} = \quad & I_l^{i,yj} \triangleleft F_\tau \tilde{C}_{46} F_{s,x} \triangleright \;+\; I_l^{i,yj} \triangleleft F_\tau \tilde{C}_{16} F_{s,z} \triangleright \;+\; I_l^{i,yj,y} \triangleleft F_\tau \tilde{C}_{56} F_s \triangleright \;+ \\
& I_l^{ij} \triangleleft F_{\tau,z} \tilde{C}_{44} F_{s,x} \triangleright \;+\; I_l^{ij} \triangleleft F_{\tau,z} \tilde{C}_{14} F_{s,z} \triangleright \;+\; I_l^{ij} \triangleleft F_{\tau,x} \tilde{C}_{24} F_{s,x} \triangleright \;+ \\
& I_l^{ij} \triangleleft F_{\tau,x} \tilde{C}_{21} F_{s,z} \triangleright \;+\; I_l^{ij,y} \triangleleft F_{\tau,z} \tilde{C}_{45} F_s \triangleright \;+\; I_l^{ij,y} \triangleleft F_{\tau,x} \tilde{C}_{25} F_s \triangleright
\end{aligned}
$$

$$
\begin{aligned}
K_{yx} = \quad & I_l^{ij,y} \triangleleft F_{\tau,x} \tilde{C}_{66} F_s \triangleright \;+\; I_l^{ij,y} \triangleleft F_{\tau,z} \tilde{C}_{56} F_s \triangleright \;+\; I_l^{i,yj} \triangleleft F_\tau \tilde{C}_{43} F_{s,z} \triangleright \;+ \\
& I_l^{i,yj} \triangleleft F_\tau \tilde{C}_{23} F_{s,x} \triangleright \;+\; I_l^{i,yj,y} \triangleleft F_\tau \tilde{C}_{36} F_s \triangleright \;+\; I_l^{ij} \triangleleft F_{\tau,x} \tilde{C}_{46} F_{s,x} \triangleright \;+ \\
& I_l^{ij} \triangleleft F_{\tau,x} \tilde{C}_{26} F_{s,x} \triangleright \;+\; I_l^{ij} \triangleleft F_{\tau,z} \tilde{C}_{45} F_{s,z} \triangleright \;+\; I_l^{ij} \triangleleft F_{\tau,z} \tilde{C}_{25} F_{s,x} \triangleright
\end{aligned}
$$

$$
\begin{aligned}
K_{yy} = \quad & I_l^{ij} \triangleleft F_{\tau,x} \tilde{C}_{66} F_{s,x} \triangleright \;+\; I_l^{ij} \triangleleft F_{\tau,x} \tilde{C}_{56} F_{s,z} \triangleright \;+\; I_l^{ij} \triangleleft F_{\tau,z} \tilde{C}_{56} F_{s,x} \triangleright \;+ \\
& I_l^{ij} \triangleleft F_{\tau,z} \tilde{C}_{55} F_{s,z} \triangleright \;+\; I_l^{ij,y} \triangleleft F_{\tau,x} \tilde{C}_{36} F_s \triangleright \;+\; I_l^{ij,y} \triangleleft F_{\tau,z} \tilde{C}_{35} F_s \triangleright \;+ \\
& I_l^{i,yj} \triangleleft F_\tau \tilde{C}_{36} F_{s,x} \triangleright \;+\; I_l^{i,yj} \triangleleft F_\tau \tilde{C}_{35} F_{s,z} \triangleright \;+\; I_l^{i,yj,y} \triangleleft F_\tau \tilde{C}_{33} F_s \triangleright
\end{aligned}
$$

$$
\begin{aligned}
K_{yz} = \quad & I_l^{ij} \triangleleft F_{\tau,x} \tilde{C}_{46} F_{s,x} \triangleright \;+\; I_l^{ij} \triangleleft F_{\tau,x} \tilde{C}_{16} F_{s,z} \triangleright \;+\; I_l^{ij} \triangleleft F_{\tau,z} \tilde{C}_{45} F_{s,x} \triangleright \;+ \\
& I_l^{ij} \triangleleft F_{\tau,z} \tilde{C}_{15} F_{s,z} \triangleright \;+\; I_l^{ij,y} \triangleleft F_{\tau,x} \tilde{C}_{56} F_s \triangleright \;+\; I_l^{ij,y} \triangleleft F_{\tau,z} \tilde{C}_{55} F_s \triangleright \;+ \\
& I_l^{i,yj} \triangleleft F_\tau \tilde{C}_{43} F_{s,x} \triangleright \;+\; I_l^{i,yj} \triangleleft F_\tau \tilde{C}_{13} F_{s,z} \triangleright \;+\; I_l^{i,yj,y} \triangleleft F_\tau \tilde{C}_{35} F_s \triangleright
\end{aligned}
$$

$$K_{zx} = \quad I_l^{i,yj} \triangleleft F_\tau \tilde{C}_{45} F_{s,z} \triangleright \quad + \quad I_l^{i,yj} \triangleleft F_\tau \tilde{C}_{25} F_{s,x} \triangleright \quad + \quad I_l^{i,yj,y} \triangleleft F_\tau \tilde{C}_{56} F_s \triangleright \quad +$$

$$I_l^{ij} \triangleleft F_{\tau,x} \tilde{C}_{44} F_{s,z} \triangleright \quad + \quad I_l^{ij} \triangleleft F_{\tau,x} \tilde{C}_{24} F_{s,x} \triangleright \quad + \quad I_l^{ij} \triangleleft F_{\tau,z} \tilde{C}_{21} F_{s,x} \triangleright \quad +$$

$$I_l^{ij} \triangleleft F_{\tau,z} \tilde{C}_{14} F_{s,z} \triangleright \quad + \quad I_l^{ij,y} \triangleleft F_{\tau,x} \tilde{C}_{46} F_s \triangleright \quad + \quad I_l^{ij,y} \triangleleft F_{\tau,z} \tilde{C}_{16} F_s \triangleright$$

$$K_{zy} = \quad I_l^{i,yj} \triangleleft F_\tau \tilde{C}_{56} F_{s,x} \triangleright \quad + \quad I_l^{i,yj} \triangleleft F_\tau \tilde{C}_{55} F_{s,z} \triangleright \quad + \quad I_l^{i,yj,y} \triangleleft F_\tau \tilde{C}_{35} F_s \triangleright \quad +$$

$$I_l^{ij} \triangleleft F_{\tau,z} \tilde{C}_{16} F_{s,z} \triangleright \quad + \quad I_l^{ij} \triangleleft F_{\tau,z} \tilde{C}_{15} F_{s,z} \triangleright \quad + \quad I_l^{ij} \triangleleft F_{\tau,x} \tilde{C}_{46} F_{s,x} \triangleright \quad +$$

$$I_l^{ij} \triangleleft F_{\tau,x} \tilde{C}_{45} F_{s,z} \triangleright \quad + \quad I_l^{ij,y} \triangleleft F_{\tau,x} \tilde{C}_{43} F_s \triangleright \quad + \quad I_l^{ij,y} \triangleleft F_{\tau,z} \tilde{C}_{13} F_s \triangleright$$

$$K_{zz} = \quad I_l^{i,yj} \triangleleft F_\tau \tilde{C}_{45} F_{s,x} \triangleright \quad + \quad I_l^{i,yj} \triangleleft F_\tau \tilde{C}_{15} F_{s,z} \triangleright \quad + \quad I_l^{i,yj,y} \triangleleft F_\tau \tilde{C}_{55} F_s \triangleright \quad +$$

$$I_l^{ij} \triangleleft F_{\tau,x} \tilde{C}_{44} F_{s,x} \triangleright \quad + \quad I_l^{ij} \triangleleft F_{\tau,x} \tilde{C}_{14} F_{s,z} \triangleright \quad + \quad I_l^{ij} \triangleleft F_{\tau,z} \tilde{C}_{14} F_{s,x} \triangleright \quad +$$

$$I_l^{ij} \triangleleft F_{\tau,z} \tilde{C}_{11} F_{s,z} \triangleright \quad + \quad I_l^{ij,y} \triangleleft F_{\tau,x} \tilde{C}_{45} F_s \triangleright \quad + \quad I_l^{ij,y} \triangleleft F_{\tau,z} \tilde{C}_{15} F_s \triangleright$$